ELSEVIER

Cardiovascular Research 69 (2006) 98 – 106

Cardiovascular Research

www.elsevier.com/locate/cardiores

Near-threshold field stimulation: Intramural versus surface activation

Christian W. Zemlin, Sergey Mironov, Arkady M. Pertsov *

Deparment Pharmacology, SUNY Upstate Medical University, 750 E Adams Street, 13210 Syracuse, NY, United States

Received 28 February 2005; received in revised form 22 July 2005; accepted 18 August 2005
Available online 13 October 2005
Time for primary review 23 days

Abstract

Objective: The mechanism by which an electric field terminates arrhythmias continues to puzzle investigators. Existing experimental methods provide information about epicardial manifestations of electrical cardioversion, yet little is known about field effects deep inside the myocardium. Here we combine specially designed optical mapping experiments and computer modeling to separate the intra-myocardial and surface field effects.

Methods: We used isolated coronary perfused and superfused slabs of pig right ventricular wall ($n=6$) stained with di-4-ANNEPS. A uniform transmural field was produced via two parallel planar (5×5 cm) transparent mesh electrodes aligned with the endocardial and epicardial surfaces. Low-intensity shocks (≤3.3 V/cm) were applied during diastole. The electrical activity under both electrodes was recorded simultaneously using two CCD cameras at 800 frames/s. Shock responses were also simulated using a bidomain Luo–Rudy model.

Results: We discovered that during the near-threshold diastolic field stimulation, when surface polarization should be dominant, the early activation occurs not at the cathodal surface, as might be expected, but deep inside the myocardium. Comparison of epi- and endocardial activation delays suggests that the sites of early activation are located closer to the endocardium. Our experimental observations could be reproduced computationally by assuming large resistive heterogeneities inside the myocardial wall.

Conclusions: Surface polarization plays a minor role during field stimulation. Intramural virtual electrodes produced even by weak fields are sufficiently strong to initiate intra-myocardial excitation. Significant heterogeneities in tissue resistivity may explain the strength of the virtual electrodes.

Keywords: Defibrillation; Excitation; Virtual electrodes; Optical mapping; Voltage-sensitive dyes

1. Introduction

A century after the invention of defibrillation [1] its mechanism remains a subject of intense debate [2]. The development of optical mapping produced a surge of new experimental information regarding the epicardial manifestations of an electric shock [3–11]. However, direct evaluation of the intramural effects of electric fields remains a major challenge on the way to resolving the puzzle of defibrillation.

All existing theories of defibrillation agree that electric fields interrupt multiple reentry circuits by simultaneously activating the bulk of the myocardium. Such activation is achieved by generating multiple virtual electrodes—alternating areas of hyper- and depolarization—inside the myocardium. Earlier studies have provided a framework for the study of shock effects [12–18] and identified several possible mechanisms, e.g. polarization of the clefts between myocardial bundles [12,19], fiber curvature [16], and cell boundaries ("sawtooth effect") [14], but the relative contributions of each mechanism to the activation of a real myocardial wall have yet to be determined.

The goal of this study is to compare the contributions of intramural virtual electrodes (IVEs) and surface polarization (SP), which occurs at the tissue-bath interface. According to all existing theories, the amplitude of SP is larger than the amplitude of IVEs [14,17,20–22]. However, the exact relationship between the amplitude of SP and amplitudes of IVEs is not known. Revealing this relationship is important to understand the mechanism of

* Corresponding author. Tel.: +1 315 464 7986; fax: +1 315 464 8014.
E-mail address: pertsova@upstate.edu (A.M. Pertsov).

0008-6363/$ - see front matter © 2005 European Society of Cardiology. Published by Elsevier B.V. All rights reserved.
doi:10.1016/j.cardiores.2005.08.012

defibrillation. SP can be measured using optical mapping and it can therefore be used as a reference for assessing the magnitude of virtual electrode effects that cannot yet be measured directly.

Our experimental approach differs from earlier studies because it combines the following elements: 1) the electric field was applied during diastole; 2) the field amplitudes were near-threshold; 3) the optical recordings were taken simultaneously from the endocardial and epicardial surfaces. As in earlier studies [5,6,23], we used coronary perfused and superfused slabs; in our case they were isolated from pig RV. To achieve a uniform transmural field, we used a pair of large planar mesh electrodes, as described earlier [5]. Combining small field amplitudes and diastolic stimulation was intended to separate SP from IVEs. If SP were a dominating factor, near-threshold fields should induce activation on only one of the myocardial surfaces, namely the one under the cathode. The surface under the anode should be activated after a significant delay dependent on the velocity of transmural propagation.

To test this hypothesis, we recorded electrical activity simultaneously from epi- and endocardium and measured activation delays at both surfaces. By comparing the delays at the sites of earliest activation on the endocardium and the epicardium, we assessed the relative proximity of primary activation sites to the surfaces. Our main finding is that the primary activation at near-threshold fields does not occur near the cathodal surface but deep inside the myocardial wall. This suggests that the amplitude of IVEs is larger than SP. To explore ways of reconciling this experimental finding with existing theories, we conducted computational studies that assess the impact of several parameters on the relative amplitude of SP and IVEs.

2. Methods

2.1. Experiments

All experimental protocols conformed to the "Guide for the Care and Use of Laboratory Animals" (NIH publication No. 85-23, revised 1996). Young pigs (15–20 kg, $n=6$) were heparinized (500 IU, IV) and subsequently anesthetized with sodium pentobarbital (35 mg/k IV). The heart was rapidly removed and Langendorff-perfused with cold (4 °C) cardioplegic solution [24]. The right free ventricular wall was quickly excised, and the right coronary artery was cannulated. Non-perfused tissue was removed, leaving a preparation of typically 5×5 cm and a thickness of 8 mm. The preparation was stretched on a plastic frame between two specially designed mesh electrodes (wire spacing was 2 mm in y-direction and 6 mm in z-direction). This electrode design provided a uniform field: The potential in the field direction dropped approximately linearly (Fig. 1A), the potential changes in the direction parallel to the electrodes are less than 10% between center and edge of the electrodes (Fig. 1B), and we observe a linear current–voltage relationship that does not depend on field polarity (Fig. 1C). Throughout the paper, we provide average field amplitudes, i.e. the potential difference between the electrodes divided by the distance between them. The field inside the tissue varies with the local tissue geometry, but is generally higher than the averaged field because the conductivity of tissue is lower than that of Tyrode solution.

The preparation was perfused with a standard oxygenated Tyrode solution [25] at 80 mm Hg and 37 °C and superfused with the same solution at a rate of 40 ml/min. We added diacetyl-monoxime (DAM) to the Tyrode solution (15 mmol/l) to stop contractions. We allowed 20 min for the preparation to equilibrate. The dye di-4-ANEPPS (15 μg/ml, from Molecular Probes), which stains for transmembrane voltage, was added as described elsewhere [26]. To monitor the state of our preparation, we measured at each pixel the action potential duration, a sensitive indicator of ischemic damage to the heart. We also recorded the transmural conduction time, which would change if the condition of the mid-myocardium deteriorated. Data were used only when both action potential duration and transmural conduction time did not differ from their initial values by more than 10%.

The optical mapping setup consisted of 2 DALSA video imaging systems for simultaneous imaging of the endo- and epicardial surfaces of the preparation. The magnification and field of view of both video cameras were adjusted such that they observed the same area (2×2 cm) of the

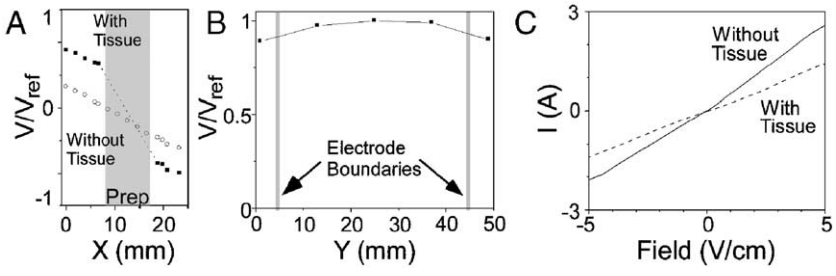

Fig. 1. Potential distribution and currents in the experimental chamber during shock application. A: Potential distribution between the electrodes during test shock in the presence of tissue (marked by "■") and the absence of tissue (marked by "○"). Shock strength was adjusted to produce equal currents with and without tissue. B: Potential distribution in the plane parallel to the electrodes, at $\Delta x=10$ mm distance from the electrodes. We show the potential distribution during a rectangular reference shock in the presence of tissue. The grey lines indicate the boundaries of the electrode. C: Current through the electrodes as a function of field strength with and without preparation for both polarities. Shock duration was 5 ms.

preparation from opposite sides. The preparation was illuminated with four 400 W tungsten halogen light sources whose light was filtered through 520±40 nm band pass filters. The fluorescent light was isolated using 640±50 nm band pass filters and recorded by the cameras.

The video images (64 × 64 pixels) were acquired at 800 frames per second, and the background fluorescence was subtracted from each frame. We used ensemble averaging to reduce noise, i.e. we averaged the epifluorescence signal from 70 sequential recordings. The signal was spatially filtered with a 5 × 5 mean filter and normalized to the local maximum amplitude. When preparing activation maps, the activation time was defined as the time between the beginning of the shock and the moment at which the transmembrane potential rose above AP_{90}.

We periodically applied shocks of rectangular waveform, 5 ms duration, and variable amplitude during the resting state at a frequency of 2 Hz. For each preparation, we determined the excitation threshold (typically 0.4–0.5 V/cm), and recorded the tissue response to shocks with an amplitude slightly above the excitation threshold for both polarities. We also recorded shocks for $E = \pm 1.1$, ±2.2, and ±3.3 V/cm. Between recordings, we continued to stimulate at 2 Hz and at a low amplitude (1.1 V/cm).

2.2. Bidomain simulations

We used a bidomain model [27] to simulate the electrical activity in response to field stimulation inside a slab of myocardial tissue immersed in a bath. The thickness of the model slab was 8 mm, similar to the RV preparations in our experiments. We assumed that cells are oriented with their long axis parallel to the surface. In this geometry, action potential propagation occurs transversely to the cells' axes. The intracellular and extracellular transversal conductivities were set at $g_i = 0.0263$ S/m and $g_e = 0.1087$ S/m, respectively [22], which lie in the range determined by experimental measurement [28–30]. The bath was assigned a conductivity of 2.0 S/m, similar to that of Tyrode solution [31].

The clefts that separate myocardial bundles [32] were incorporated into our model by lowering the transversal conductivity to $g_c < g_I$ randomly every 2 to 8 cells, corresponding to bundle thicknesses of 30–120 μm. For $g_c = 0.1 g_i$, the SP amplitude was about 2.5 times the size of the largest intramural electrodes, similar to what has been reported previously [22]. Consequently, we used this g_c as our standard cleft conductivity. To reproduce our experimental results, we reduced g_c to 0.036 g_i and introduced a large heterogeneity in the medium (see Results). Concurrently with any change in g_c, we adapted g_i to keep the propagation velocity constant.

Since the fields we apply were directed transmurally, we assumed that all induced currents were also directed transmurally. This allowed us to treat the electrical activity in our slab in one dimension, similarly to Refs. [10,11,22]. We computed the transmembrane currents using the Luo–Rudy II dynamic model [33] To discretize the model, we used a time step between 0.5 and 5 μs and a space step of 17 μm, corresponding to a total of 483 cells across our model myocardial wall.

3. Results

3.1. Near-threshold field stimulation in perfused RV slabs

Fig. 2 shows the effect of a near-threshold field ($E = 0.4$ V/cm) applied to a slab of tissue during the

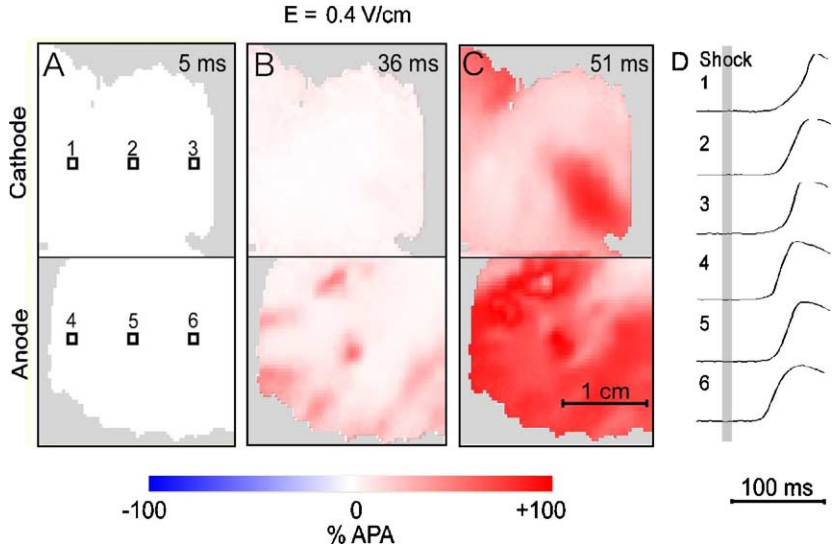

Fig. 2. Effect of near-threshold fields applied during the resting state. A-C: Color-coded distribution of transmembrane voltage at different times for a field E=0.4 V/cm. Color bar at the bottom shows meaning of colors, grey pixels were not mapped. Time elapsed since beginning of shock is shown in the upper right-hand corner. Numbered boxes in Panel A indicate locations of upstroke recordings (see Panel D). D: Fluorescence upstrokes during and after the shock, recorded from anodal and cathodal surface (from locations given in Panel A).

resting state. Panels A–C show the distribution of transmembrane voltage on both surfaces after the shock. At the end of the shock both surfaces are still uniformly at resting potential (Panel A). The response appears only after a substantial delay (Panel B). Red spots at the anodal surface show the areas of depolarization (breakthroughs). Such areas are still absent on the cathodal surface, which is activated significantly later (Panel C). The absence of polarization during the shock and the delayed activation of both surfaces suggest that the primary activation induced by the shock occurred inside the myocardial wall. Panel D shows optical upstrokes from selected locations indicated in Panel A. Some of the optical upstrokes have a slow foot (see traces 1 and 3), characteristic of wave fronts moving towards the recording surface [34]. This provides additional evidence for the intramural origin of the primary activation. Results similar to those shown in Fig. 2 were observed in all six preparations.

By comparing the earliest activation times on the epicardial (τ_{epi}) and endocardial (τ_{endo}) surfaces during near-threshold diastolic shocks, we estimated the location of the site of the early activation inside the myocardial wall (assuming constant transmural propagation velocity). See the Discussion section for the limitations of this approach. Table 1 shows the ratios τ_{epi}/τ_{endo} for all preparations, with the anode at the epicardium. While τ_{endo} ranged from 6.6 to 29.6 ms, the values of τ_{epi}/τ_{endo} generally lay in the narrow interval from 1.0 to 1.5 (with one exception). A ratio τ_{epi}/τ_{endo} greater than unity indicates that the epicardium was activated after the endocardium and therefore suggests that the primary activation was closer to the endocardium. Ratios between 1.0 and 1.5 correspond to primary activation sites between 40% and 50% of the way through the myocardial wall, starting from the endocardium.

It is interesting that the ratio τ_{epi}/τ_{endo} did not significantly depend on field polarity. When we reversed the field polarity in four preparations (anode at endocardium, see Table 2), the epicardial activation time remained longer or equal in all cases, with τ_{epi}/τ_{endo} now ranging from 1.0 to 2.0. This means that the endocardial activation time was shorter than the epicardial activation time independently of the polarity of the stimulating field. Moreover, τ_{epi}/τ_{endo} had a similar value in three out of four preparations (prep. 1, 2, and 3). This shows that the depth of primary activation is approximately the same independently of the polarity of the stimulating field.

Table 1
Surface activation times at near-threshold fields Anode at epicardium

Prep#	1	2	3	4	5	6
τ_{epi}/τ_{endo}	1.4	1.4	1.0	7.7	1.1	1.5
τ_{endo} (ms)	15.4	29.6	13.2	7.7	11.0	6.6

Abbreviations are as defined in the text.

Table 2
Surface activation times at near-threshold fields Cathode at epicardium

Prep#	1	2	3	4
τ_{epi}/τ_{endo}	1.3	1.4	1.0	2.0
τ_{endo} (ms)	16.4	20.8	9.9	7.7

Abbreviations are as defined in the text.

3.2. Effect of field strength

Higher field intensity resulted in significantly more breakthrough sites, smaller activation delays, and reduced dispersion of the activation times. Fig. 3A shows the cathodal (epicardium) and anodal (endocardium) color-coded activation maps after diastolic field application in one of the preparations. We varied the field intensity from near-threshold (0.4 V/cm) to more than eight times threshold (3.3 V/cm). For threshold stimulation (left panel), one can clearly identify early activation sites (green) at corresponding locations on both surfaces. The activation occurred after a significant delay (12 ms) almost simultaneously under cathode and anode. This suggests that primary activation originated approximately in the middle of the myocardial wall. Progressive increases in shock intensity resulted in a significant reduction of delays and reduced dispersion of activation times (the color of the activation map shifted from yellow to blue and then to purple; at the same time, it became more uniform).

To further quantify the data presented in Fig. 3A we plotted the distributions of the activation times for each of the activation maps (see Fig. 3B). With increasing shock amplitude the distributions became narrower (notice the different ranges of the x-axes) and the mean shifted towards lower delays. Even for the weakest shocks, the time difference between earliest and latest activation was only 13 ms at the anode and 15 ms at the cathode. This time is too short for propagation of excitation through the field of view (2.8 cm), which confirms that we are looking at a breakthrough pattern.

The effects we observed when varying field strength in all our preparations are summarized in Fig. 4. The mean activation time, averaged over all preparations, declined sharply when the shock amplitude was increased from E=0.4 to 1.1 V/cm (see Fig. 4A), continued to decrease with increasing shock strength, and leveled out at about 4 ms for E=3.3 V/cm. There was no significant difference between anodal and cathodal values. Similarly, the standard deviation of the activation time decreased sharply from E=0.4 to 1.1 V/cm and went down to practically 0 for E=2.2 and 3.3V/cm (see Fig. 4B), indicating simultaneous activation of each surface. In addition to these changes, we also observed significantly faster optical upstrokes (not shown). Taken together, these data suggest that with increasing shock amplitude, the intra-myocardial areas of primary activation expand significantly and approach the surface.

It is interesting that we did not observe hyperpolarization near the anodal surface for any of the amplitudes tested.

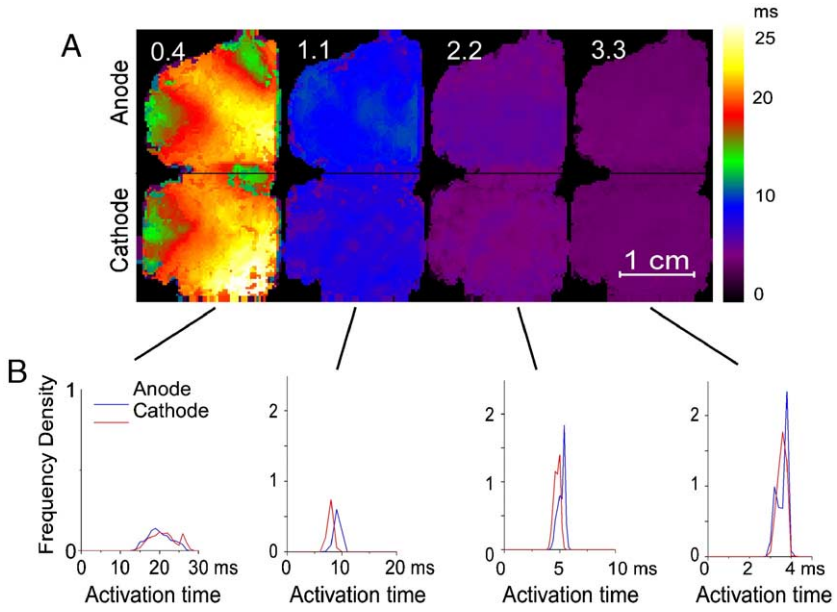

Fig. 3. Epi-and endocardial activation after diastolic field stimulation (cathode on epicardium). A: Color-coded activation maps for epi-and endocardium (see color bar to the right for the meaning of colors). The white number in the upper left-hand corner of images indicates field amplitude in V/cm. B: Frequency densities of anodal (blue) and cathodal (red) activation times for different field amplitudes for the experiment illustrated in Panel A.

Fig. 5 shows the time dependence of the cathodal and anodal polarization during the diastolic shocks of 0.4 V/cm and 3.3 V/cm (averaged over all 6 experiments). To quantify the degree of anodal and cathodal polarization during the shock, we averaged the optical signal spatially over the whole preparation and subtracted the resting potential (average of 20 ms interval before the shock) from the transmembrane potential at each surface during the shock. For fields of 0.4 V/cm (see Fig. 5A), the polarization was not significantly different from zero at any moment during

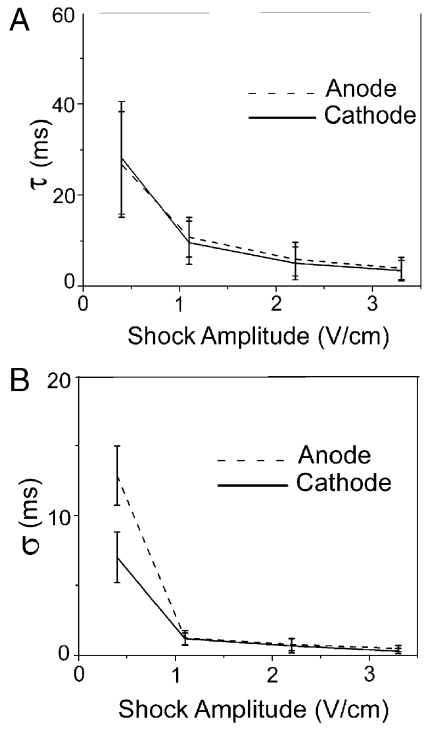

Fig. 4. Mean activation time (A) and standard deviation (B) of activation time as a function of field amplitude, averaged over all preparations. Error bars indicate the standard deviation.

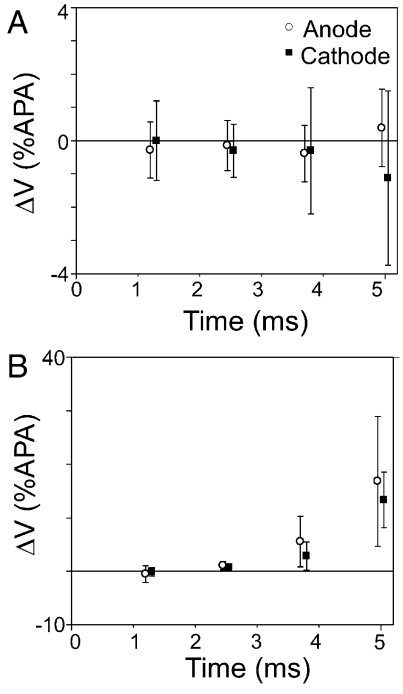

Fig. 5. Anodal and cathodal polarization amplitude during diastolic field stimulation. A: Near-threshold stimulation (E=0.4 V/cm). Average SP ΔV as a function of time after the onset of the shock. Amplitudes have been averaged over all preparations, error bars indicate standard deviations. B: The same at field strength E=3.3 V/cm.

the shock, neither under the anode nor under the cathode. This amplitude was, however, strong enough to initiate excitation inside the wall, suggesting that the amplitude of IVEs is significantly larger than that of SP. For stronger fields (3.3 V/cm), in 5 out of 6 experiments we observed depolarization both under the cathode and anode. The level of depolarization was similar on both surfaces and reached significant values (up to 20% of the action potential amplitude) by the end of the shock, suggesting the onset of activation well before the shock ended.

3.3. Bidomain simulations

To get a better understanding of the relative relationship between SP and IVEs, we simulated shocks in a Luo-Rudy [33] bidomain model [27] in which we incorporated the bundled structure of the myocardial wall (see Methods).

As anticipated, for standard parameters (see Methods section) field stimulation near the threshold produced activation at the cathodal surface that subsequently spread towards the anode. The field stimulation threshold was 0.6 V/cm, consistent with an earlier bidomain simulation [31] One such simulation is illustrated in Fig. 6A, B. The jagged trace in Fig. 6A shows the distribution of the transmembrane voltage across the myocardial wall during the shock (1 ms after its onset). Small-wavelength variations of the transmembrane voltage are IVEs produced by the shock at the clefts between muscle bundles ("bundle sawtooth"). For the most part, virtual electrodes have amplitudes of only a few millivolts, which is significantly smaller than the SP. Right after the shock (t=6 ms), SP at the cathode has grown enough to excite the tissue at the cathode and initiate a traveling wave; at the same time, the voltage distribution becomes smooth because the IVEs disappear. At t=15 ms, the excitation wave (dashed line) has traversed about one third of the wall towards the anode. The conduction velocity was highly uniform (R=-0.998 for one direction in a space-time plot and R=0.997 for the opposite direction).

Fig. 6B shows shock-induced action potentials at the cathodal and anodal surfaces. At the cathode, the action potential starts almost immediately after the onset of the shock (dashed line). A positive deflection apparent during the shock is due to SP. At the anode, the action potential appears after a significant delay (t=38 ms) that reflects the conduction time from the site of primary activation at the cathodal surface to the anode. A negative deflection during the shock reflects the negative SP.

This simulation is fully consistent with earlier simulation studies [22,35] which predict that the amplitude of SP exceeds that of the IVEs by far. However, it is in apparent disagreement with our experimental observations, which suggest that the amplitude of IVEs can exceed that of the SP. To address this discrepancy, we analyzed which parameters can affect the relationship between the amplitude of SP and IVEs. Our analysis shows that one such parameter is the cleft conductivity. By decreasing this conductivity, we were able to decrease the ratio of SP to IVE amplitudes significantly.

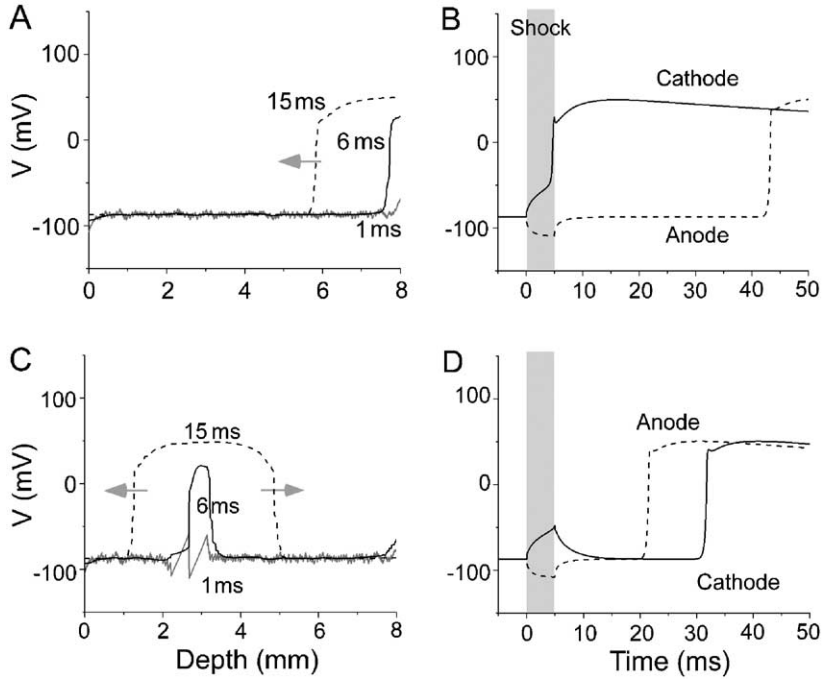

Fig. 6. Computer simulation of intramyocardial activation produced by near-threshold field stimuli. A-B: Transmural propagation of excitation initiated by a shock for standard parameters ($g_c=0.1g_i$). A: Transmural voltage profiles at 1, 6, and 15 ms after the onset of the shock. The excitation starts at the cathode (8 mm). The arrow indicates the direction of propagation of the initiated wave. B: Electrical surface signals for both surfaces of the preparation. C-D: Intramural activation for lower transmural conductivity ($g_c=0.036g_i$). Details as in Panel A-B.

Fig. 6C and D show results of a simulation similar to the one shown in Fig. 6A and B, with the cleft conductivity decreased from $0.1g_i$ to $0.036g_i$ and an especially large heterogeneity added at a depth of about 2.5 mm (with $g_c=0.012g_i$ and bundles of 0.4 mm thickness at each side). Comparing with Fig. 6, one can clearly see the reduced amplitude of SP and the increased amplitude of IVEs. The amplitude of the largest intramural virtual electrode, located at the depth 2.5 mm, exceeds the amplitude of SP. Accordingly, right after the shock (t=6 ms), we observe no traveling wave starting from the cathodal surface, but instead from an intramural virtual electrode. At t=15 ms, the excited region has widened symmetrically from the site of primary activation.

The calculated electrical surface signals for the simulation with decreased cleft conductivity are shown in Fig. 6D. The action potentials on both surfaces develop after a significant delay. The anodal surface is activated at t=20 ms and the cathodal surface at t=32 ms. Thus, the model with decreased cleft conductivity can reproduce the activation sequences that we observed in our experiments.

4. Discussion

4.1. Intramural versus SP

Our main finding is that near-threshold diastolic shocks consistently excite tissue inside the myocardium. This finding challenges the predictions of current theories of defibrillation, which imply that the shock effect should be maximal near the cathodal surface. The predicted ratio of the amplitudes of SP and IVEs varies significantly between models. The largest reported values range from 10 in the Plonsey-Barr model [14] to about 5 in a dynamic 1D model by Keener [17]. Lower values are reported for more recent, detailed models by Entcheva et al. [20]. Efimov et al. [21], and Hooks et al. [22] (a value of 2.5 in the case of Hooks). All models agree that the SP amplitude is significantly larger than that of IVEs.

To date there have been only few experimental reports in which the electrical field was applied during the diastole and none of them used near-threshold field strengths; this makes it difficult to directly compare our observations with earlier studies. Yet, by analyzing earlier reports one can find indirect evidence supporting our conclusion. In particular, data presented by Sharifov and Fast [7] exhibit IVE-induced activation without full depolarization of the cathodal surface. Similarly to our findings, this observation does not agree with current theories, which predict that the surface effect of a shock should be dominant. Indeed, if the ratio of the amplitude of SP to that of IVEs were as high as predicted, a field strength sufficient to induce intramural excitation should be more than sufficient to fully depolarize the cathodal surface.

Additional experimental evidence against the dominant role of SP comes from the analysis of the dependence of surface activation delay on shock strength. Both in our experiments (see Fig. 4A) and in those of Sharifov and Fast [7], this activation delay rapidly decreases with increasing shock amplitude. Again, this is not what one would expect from the existing theories. If SP were dominant, there should be a broad range of shock amplitudes which are strong enough to activate the cathodal surface, but too weak to initiate activation at IVEs. This should give rise to a plateau in the plot of anodal activation delay against shock amplitude. The absence of such a plateau in experiments and the observed rapid decrease of activation delays at increasing shock strength, with an increase in the number of activation sites, suggest that SP does not have a larger amplitude than IVEs.

If SP and IVEs have similar amplitudes, small differences in anatomical structure can result in distinctly different shock manifestations. In the case of slightly higher SP, shocks of threshold amplitude would excite only the cathode. Consequently, there would be a correlation between shock polarity and primary activation site. In the case of stronger IVEs, shocks of threshold amplitude should excite only the most susceptible site, which is determined by anatomy. This could explain why Sharifov and Fast have found a correlation between shock polarity and primary activation site [7] that we did not see. They used pig LV while we used pig RV, and it is reasonable to assume that due to their different anatomy, LV and RV preparations exhibit slightly different ratios of SP to IVE amplitudes. In any case, both studies suggest that SP is far less dominating than currently assumed.

4.2. Absence of anodal hyperpolarization

We did not observe any hyperpolarization under the anode during shocks applied to the resting state for the whole range of shock amplitudes up to 3.3 V/cm (Fig. 3). However, when we applied shocks during the plateau phase of an action potential in the same preparations, we observed a substantial degree of SP, consistent with previous experiments [4,5,9,21]. The lack of anodal hyperpolarization during diastolic field stimulation can be explained based on recent findings by Sharifov and Fast which suggest that hyperpolarization may be masked by a net depolarization of subsurface layers [8]. When they stained only the surface layers (thickness $\sim$100 μm), they were able to record hyperpolarization for about 2 ms (at 2 V/cm) before active depolarization caused by IVEs became dominant.

4.3. Reconciliation with theory

To explore the possibility of reconciling the theory and experiment we constructed a simple bidomain computer model of the phenomenon in question that takes into account macroscopic heterogeneities of the myocardial wall

such as clefts between bundles of myocardial cells [22,36,37]. In our simulations, reducing the coupling between myocardial bundles increased the amplitude of IVEs while it simultaneously reduced the strength of SP; a similar effect could be achieved by reducing the coupling of cells at gap junctions [38]. This result raise the question how accurate the numerical values of the conductivities used in current theories are. These values are derived from macroscopic measurements that assume continuity of the myocardium [29], while its discrete microscopic properties are included in these models only in an average way. Therefore, it is possible that the commonly used conductivities are inaccurate. To resolve this important question, new protocols have been suggested to measure the microscopic conductive properties of heart tissue [30,38]. However, these protocols have not yet been utilized to collect experimental data.

Finally, we would like to note that weak coupling alone was not sufficient to induce intramural activation in our simulations. We were able to reproduce our experimental results only after we added a large resistive heterogeneity. It is interesting that the depth of earliest intramural activation estimated it from our experiments coincides with the depth of the lowest anatomical connectivity between bundles [36]. Future studies will show whether the low connectivity is the actual cause of the activation [37].

4.4. Limitations

Both in our experiments and our simulations we used a special geometry; the preparation was planar and the field constant and perpendicular to the preparation. Polarization due to fiber curvature [16] or field inhomogeneities should not occur in this geometry, and resistive heterogeneity is the only apparent cause for virtual electrodes. While this allowed us to separate the effects of virtual electrodes due to resistive heterogeneities, shock fields used in defibrillation are not uniform and do not always have the transmural orientation. More research is needed to assess the effects of fiber curvature and inhomogeneous fields.

Our estimates of the sites of primary activation at near-threshold fields assumed a constant transmural propagation velocity. There are experimental data supporting this assumption [39], but it remains an approximation. We also did not take into account a possible latency of activation [40]. Such a latency could increase the activation times on the epicardial and endocardial surfaces equally. Finally, if several nearby locations are activated by the shock, we would at each surface record the activation delay of the closest activated location.

While we argued that the effect of the shock is particularly strong at the site of earliest activation, a transmural variation of activation threshold could also play a role in determining where the earliest activation occurs. Possible causes for such a transmural variation are the presence of Purkinje fibers, which in pigs can reach into the subendocardium, and the known variation in ionic channel density across the myocardial wall [41].

A further limitation of this study is the use of the electromechanical uncoupler DAM to suppress motion artifacts. While DAM is known to affect ionic currents and the action potential duration [42], it does not significantly change the resting potential, the maximum upstroke velocity, or the action potential amplitude [41], and should therefore have no significant influence on any of the results we reported.

Acknowledgments

We thank Olivier Bernus, Marcel Wellner, and Arvydas Matiukas for useful discussions and Marcel Wellner and Charles Danko for carefully reading the manuscript. Research in this article has been supported by AHA grant #0325458T and by NIH grants 5P01HL039707, 5R01HL071635, and 5R01HL071762.

References

[1] Prevost JL, Batelli F. La Mort Par Les Descharges Electriques. J Physiol 1899;1:1085–100.
[2] Mackenzie D. Making sense of a heart gone wild. Science 2004; 303:786–7.
[3] Dillon SM. Synchronized repolarization after defibrillation shocks. A possible component of the defibrillation process demonstrated by optical recordings in rabbit heart. Circulation 1992;85:1865–78.
[4] Fast VG, Sharifov OF, Cheek ER, Newton JC, Ideker RE. Intramural virtual electrodes during defibrillation shocks in left ventricular wall assessed by optical mapping of membrane potential. Circulation 2002;106:1007–14.
[5] Sharifov OF, Fast VG. Intramural virtual electrodes in ventricular wall: effects on epicardial polarizations. Circulation 2004;109: 2349–56.
[6] Sharifov OF, Ideker RE, Fast VG. High-resolution optical mapping of intramural virtual electrodes in porcine left ventricular wall. Cardiovasc Res 2004;64:448–56.
[7] Sharifov OF, Fast VG. Optical mapping of transmural activation induced by electrical shocks in isolated left ventricular wall wedge preparations. J Cardiovasc Electrophysiol 2003;14:1215–22.
[8] Sharifov O, Fast V. Role of intramural virtual electrodes in electric shock-induced transmural activation of porcine left ventricle assessed optically from intact epicardial surface (abstract). Heart Rhythm Journal, vol. 2. 2005. p. S258 [Abstract].
[9] Zhou X, Ideker RE, Blitchington TF, Smith WM, Knisley SB. Optical transmembrane potential measurements during defibrillation-strength shocks in perfused rabbit hearts. Circ Res 1995;77:593–602.
[10] Efimov IR, Gray RA, Roth BJ. Virtual electrodes and deexcitation: new insights into fibrillation induction and defibrillation. J Cardiovasc Electrophysiol 2000;11:339–53.
[11] Chattipakorn N, Banville I, Gray RA, Ideker RE. Mechanism of ventricular defibrillation for near-defibrillation threshold shocks: a whole-heart optical mapping study in swine. Circulation 2001;104: 1313–9.
[12] Sobie EA, Susil RC, Tung L. A generalized activating function for predicting virtual electrodes in cardiac tissue. Biophys J 1997; 73:1410–23.
[13] Roth BJ. Mechanisms for electrical stimulation of excitable tissue. Crit Rev Biomed Eng 1994;22:253–305.

[14] Plonsey R, Barr RC. Effect of microscopic and macroscopic discontinuities on the response of cardiac tissue to defibrillating (stimulating) currents. Med Biol Eng Comput 1986;24:130–6.
[15] Trayanova N, Pilkington TC. A bidomain model with periodic intracellular junctions: a one-dimensional analysis. IEEE Trans Biomed Eng 1993;40:424–33.
[16] Trayanova N, Skouibine K, Aguel F. The role of cardiac tissue structure in defibrillation. Chaos 1998;8:221–33.
[17] Keener JP. Direct activation and defibrillation of cardiac tissue. J Theor Biol 1996;178:313–24.
[18] Krinsky V, Pumir A. Models of defibrillation of cardiac tissue. Chaos 1998;8:188–203.
[19] Fast VG, Rohr S, Gillis AM, Kleber AG. Activation of cardiac tissue by extracellular electrical shocks: formation of 'secondary sources' at intercellular clefts in monolayers of cultured myocytes. Circ Res 1998;82:375–85.
[20] Entcheva E, Eason J, Efimov IR, Cheng Y, Malkin R, Claydon F. Virtual electrode effects in transvenous defibrillation-modulation by structure and interface: evidence from bidomain simulations and optical mapping. J Cardiovasc Electrophysiol 1998;9:949–61.
[21] Efimov IR, Aguel F, Cheng Y, Wollenzier B, Trayanova N. Virtual electrode polarization in the far field: implications for external defibrillation. Am J Physiol Heart Circ Physiol 2000;279:H1055–70.
[22] Hooks DA, Tomlinson KA, Marsden SG, LeGrice IJ, Smaill BH, Pullan AJ, et al. Cardiac microstructure: implications for electrical propagation and defibrillation in the heart. Circ Res 2002;91:331–8.
[23] Zaitsev AV, Berenfeld O, Mironov SF, Jalife J, Pertsov AM. Distribution of excitation frequencies on the epicardial and endocardial surfaces of fibrillating ventricular wall of the sheep heart. Circ Res 2000;86:408–17.
[24] Huang AH, Sofola IO, Bufkin BL, Mellitt RJ, Guyton RA. Coronary sinus pressure and arterial venting do not affect retrograde cardioplegia distribution. Ann Thorac Surg 1994;58:1499–504.
[25] Asano Y, Davidenko JM, Baxter WT, Gray RA, Jalife J. Optical mapping of drug-induced polymorphic arrhythmias and torsade de pointes in the isolated rabbit heart. J Am Coll Cardiol 1997;29:831–42.
[26] Baxter WT, Davidenko JM, Loew LM, Wuskell JP, Jalife J. Technical features of a CCD video camera system to record cardiac fluorescence data. Ann Biomed Eng 1997;25:713–25.
[27] Henriquez CS. Simulating the electrical behavior of cardiac tissue using the bidomain model. Crit Rev Biomed Eng 1993;21:1–77.
[28] Roth BJ. Electrical conductivity values used with the bidomain model of cardiac tissue. IEEE Trans Biomed Eng 1997;44:326–8.
[29] Clerc L. Directional differences of impulse spread in trabecular muscle from mammalian heart. J Physiol 1976;255:335–46.
[30] Le Guyader P, Trelles F, Savard P. Extracellular measurement of anisotropic bidomain myocardial conductivities. Ann Biomed Eng 2001;29:862–77.
[31] Trayanova NA, Roth BJ, Malden LJ. The response of a spherical heart to a uniform electric field: a bidomain analysis of cardiac stimulation. IEEE Trans Biomed Eng 1993;40:899–908.
[32] Robb J, Robb RC. The normal heart: anatomy and physiology of the structural units. Am Heart J 1942;23:455–67.
[33] Luo CH, Rudy Y. A dynamic model of the cardiac ventricular action potential: I. Simulations of ionic currents and concentration changes. Circ Res 1994;74:1071–96.
[34] Hyatt CJ, Mironov SF, Wellner M, Berenfeld O, Popp AK, Weitz DA, et al. Synthesis of voltage-sensitive fluorescence signals from three-dimensional myocardial activation patterns. Biophys J 2003;85:2673–83.
[35] Efimov IR, Aguel F, Cheng Y, Wollenzier B, Trayanova N. Virtual electrode polarization in the far field: implications for external defibrillation. Am J Physiol Heart Circ Physiol 2000;279:H1055–70.
[36] LeGrice IJ, Smaill BH, Chai LZ, Edgar SG, Gavin JB, Hunter PJ. Laminar structure of the heart: ventricular myocyte arrangement and connective tissue architecture in the dog. Am J Physiol 1995;269:H571–82.
[37] Young AA, Legrice IJ, Young MA, Smaill BH. Extended confocal microscopy of myocardial laminae and collagen network. J Microsc 1998;192(Pt. 2):139–50.
[38] Pollard AE, Smith WM, Barr RC. Feasibility of cardiac micro-impedance measurement using multisite interstitial stimulation. Am J Physiol Heart Circ Physiol 2004;287:H2402–11.
[39] Poelzing S, Rosenbaum DS. Altered connexin43 expression produces arrhythmia substrate in heart failure. Am J Physiol Heart Circ Physiol 2004;287:H1762–70.
[40] Shibata N, Chen PS, Dixon EG, Wolf PD, Danieley ND, Smith WM, et al. Epicardial activation after unsuccessful defibrillation shocks in dogs. Am J Physiol 1988;255:H902–9.
[41] Antzelevitch C, Fish J. Electrical heterogeneity within the ventricular wall. Basic Res Cardiol 2001;96:517–27.
[42] Sellin LC, McArdle JJ. Multiple effects of 2,3-butanedione monoxime. Pharmacol Toxicol 1994;74:305–13.